<div align="right">

3

</div>

<div align="center">

Fe₃C/C nanocomposite

</div>

3.1 Introduction

The structural, magnetic and *in-vitro* analysis of the Fe_3C nanoparticles are described in this chapter. The monophasic extremely fine nanoparticles of Fe_3C were produced opting a simple and cost effective sol-gel assisted route. The physical, morphological (i.e. shape and size) and magnetic properties were studied by usual techniques. The heating performance (adiabatically) in the presence of external AC magnetic field of this carbide based aqueous ferrofluid was evaluated and compared with iron oxide based MNPs. The cytotoxicity assessments were carried out for bare nanoparticles and their ferrofluid by Sulforhodamine B assay (SRB) with human lung adenocarcinoma A549 cells.

3.2 Results and discussion

3.2.1 Phase identification by X-ray diffraction

Figure 3.1 (a) presents the X-ray diffraction pattern after the Rietveld refinement for Fe_3C, produced by the sol-gel assisted technique. The diffraction peaks of the pattern were similar to the JCPDS no. # 65-2413 for the orthorhombic iron carbide (Fe_3C). The Rietveld refinement of the diffraction pattern was accomplished by Fullprof software. The obtained structural parameters after the Rietveld refinement are shown in Table 3.1.

The crystallite size of the material was estimated to be ~ 4 nm by the Scherrer's equation. After the Rietveld refinement, the atomic positions for the iron (Fe) and carbon (C) atoms in the orthorhombic unit cell are drawn with the help of VESTA software and shown in figure 3.1 (b). The image suggests that in the orthorhombic iron carbide system, carbon was present at the octahedral interstitial voids, which are also reported in earlier works. The bond lengths between Fe-C atoms and Fe-Fe atoms were 1.621 and 4.612 Å, respectively. The bond angle between Fe-C-Fe was 39.5°. The lattice parameter and atomic positions are observed to be similar in magnitude from both the software.
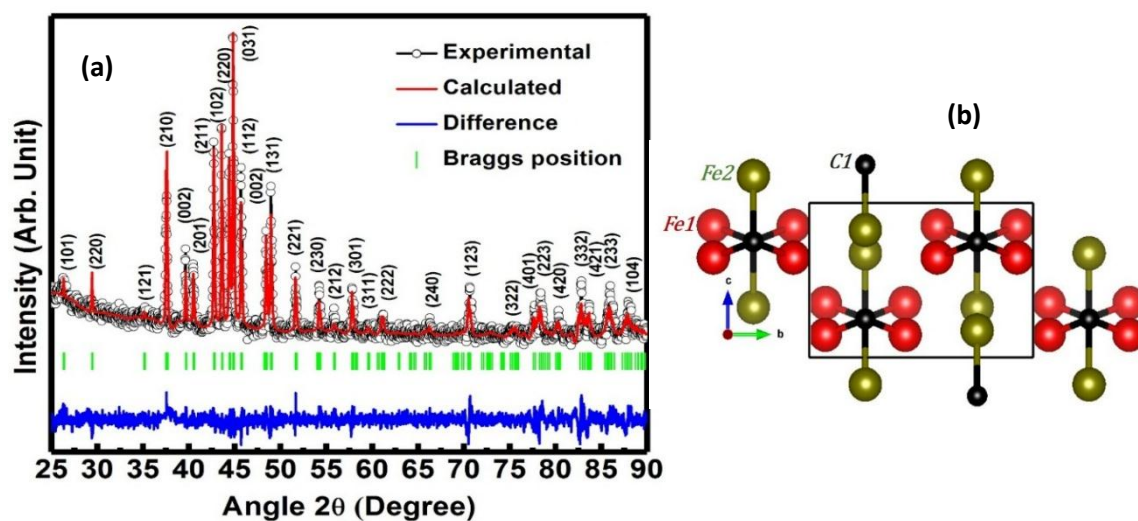

Figure 3.1: a) Rietveld refined X-ray diffraction pattern of ultrafine Fe_3C, nanoparticles and b) Atomic position of Fe and C atoms in the unit cell as obtained from VESTA

The detailed reaction mechanism for this process to achieve Fe_3C may be understood as follows. The sol-gel process used for the synthesis is based on hydrolysis and polycondensation reactions. For this purpose, the $FeCl_3$ precursor was dissolved initially in the solvent (ethanol and distilled water) which transformed it into hydroxide by hydrolysis.

Table 3.1: Obtained structural parameters of the Fe_3C nanoparticles after the Rietveld refinement.

Sample	Space group (S.G)	Lattice parameter a , b, c	α β γ	Unit cell volume $(\AA^3)$ V	Atomic position Fe1 (x, y, z)	Atomic position Fe2 (x, y, z)	Atomic position C1 (x, y, z)	Atomic occupancy (site) Fe1, Fe2, C1	χ^2
		5.0929	90		0.176	0.036	0.8893	2	1.2
Fe_3C	Pnma	6.7467	90	155.599	0.065	0.25	0.25	1	
	62	4.5285	90		0.344	0.829	0.432	1	

The organic materials such as urea (NH_2CONH_2) and cetyltrimethylammonium bromide ($C_{19}H_{42}BrN$) were dissolved into the solvent and stirred mechanically at 70 °C for 6 h. This facilitates the polycondensation reaction and produces a light brown gel. The obtained solid product was put at ~200 °C for 12 h to get the oxide phase. During this treatment, urea transformed into carbamylurea by condensation reaction giving H_2O and NH_3 as byproducts. The resulted solid was then heat treated at 700 °C in an N_2 environment for 3 h. At this condition, carbamylurea transforms into C_xN_y (graphitic carbon nitride materials), which converts oxide into carbide. Further, Br produced due to CTAB, acted as a catalyst during this reaction. It has been observed that the amount of CTAB, as well as reaction temperature, are very crucial to get a pure carbide phase. The excess amount of CTAB gives Fe as the final product, whereas for a lesser amount of it, the carburization does not complete, which results in an untransformed oxide phase [119, 148].

3.2.2 TEM analysis

The bright-field micrograph of the Fe_3C particles taken by TEM is shown in Fig. 3.2. The bright-field micrograph indicates spherical shaped particles. The inset shows

ring type SAED patterns confirming the polycrystalline nature. The SAED pattern was analyzed (eRing software) and it confirmed the Fe_3C phase as supported by the XRD study (Fig. 3.1). Following the literature, the particles were treated with 30 % H_2O_2 to remove the excess C from the surface of the particles. The range of the particle size is shown as a histogram (Fig. 3.2 b), which has been plotted based on the obtained bright-field images of the material (Fig. 3.2 a). The particle size was estimated (considering around 350 particles and using ImageJ software) to be in the range of 4 to 11 nm, and the mean size was ~ (6 ± 0.5) nm.
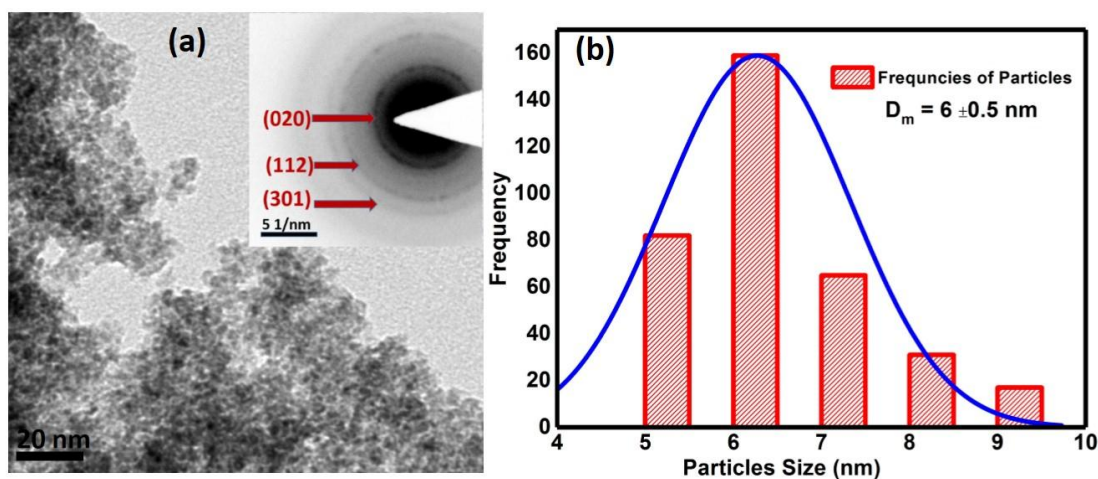

Figure 3.2: TEM analysis of Fe_3C nanoparticles (a) bright field micrograph and inset represents the SAED pattern, and (b) histogram of size distribution.

3.2.3 X-ray photoelectron spectroscopy

XPS experiment was performed to study the oxidation state of the elements present in Fe_3C MNPs. It was observed that this carbide contains Fe, C, and physically adsorbed O element over its surface (Fig. 3.3). The XPS spectrum of Fe 2p in Fig. 3.3 (b) exhibits two sharp peaks having binding energies 724.6 eV and 711.3 eV, which can be attributed to the Fe 2p1/2 and Fe 2p3/2. It indicates the presence of atomic state Fe in

Fe₃C phase. Further, a satellite peak at 714.6 eV is deconvoluted for the Fe $2p_{3/2}$ which may be ascribed to Fe^{3+} state due to surface oxidation. The spectrum of C 1s after deconvolution is shown in Fig. 3.3 (b).
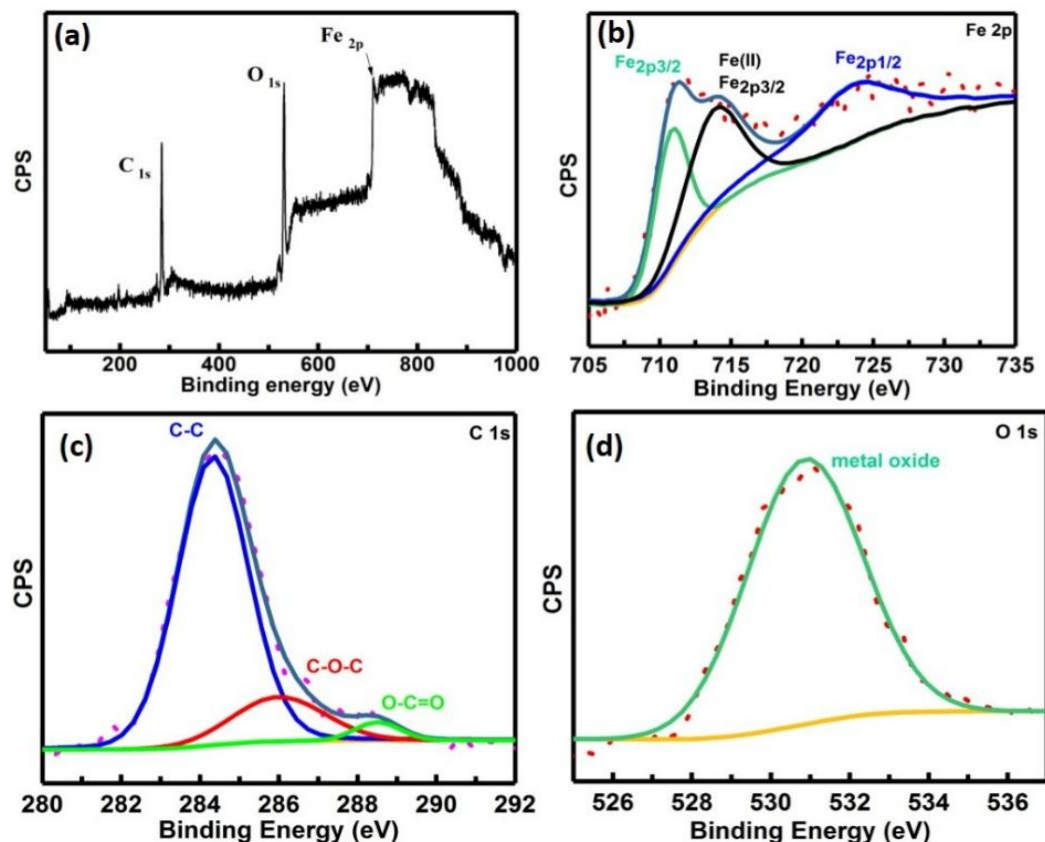

Figure 3.3: (a) The wide range of X-ray photo spectra of Fe₃C sample, (b) spectrum for Fe2p states, (c) spectrum for C 1s and (d) core level spectrum for absorbed O 1s.

The observed three peaks at 284.9, 285.73, and 288.9 represent the C-C, C-O-C, and O-C=O bonds respectively. Such bonding could be due to the adsorption of oxygen over the surface of carbide nanoparticles. The O 1s spectrum had one peak at 531.5 eV, which could be ascribed to metal-oxygen and C-O bondings (Fig. 3.3 d). The existence

of Fe and C elements in wide spectrum validates that the Fe reduced to Fe_3C MNP_S during the heat treatment process.

3.2.4 Magnetic measurement

The magnetization *vs.* field curve for as-synthesized Fe_3C material at ambiance condition is shown in Fig. 3.4, which was taken up to ± 2 T. The magnitude of the M_S was ~78 Am^2/kg, which was lesser than its bulk magnetization value (~130 Am^2/kg). The large reduction in the M_S value may be attributed to the magnetic dead layer over MNPs as well as the presence of carbon. The remanence and coercivity values for this material were found to be around 0.86 Am^2/kg, and 1.95 mT, respectively.
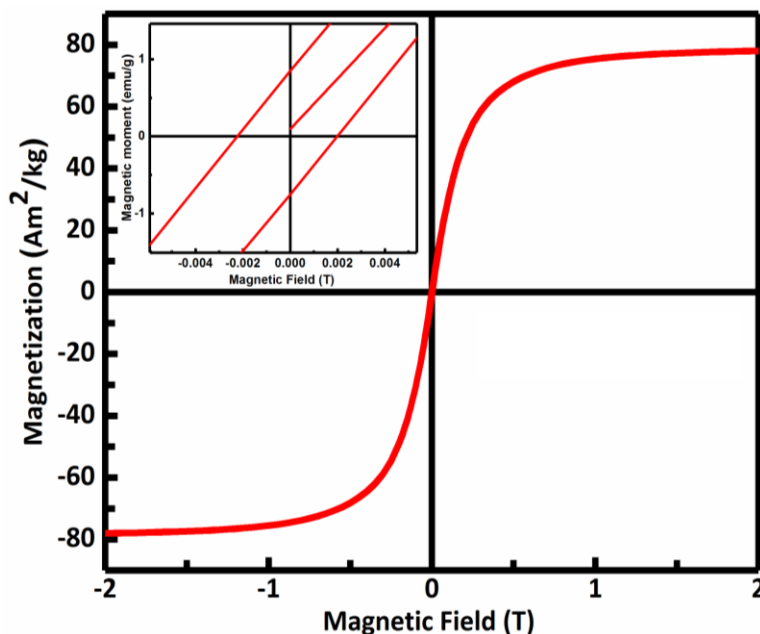

Figure 3.4: The M *vs.* H plot for as-synthesized Fe_3C magnetic nanoparticles.

Nevertheless, the magnitude of M_S was comparatively more significant than that of the similar sized iron oxides nanoparticles (40-60 Am^2/kg). The M_S value obtained was even more than the reported values, as the earlier reported samples had carbon

coating over their surface. Moreover, the values of M_S, M_r, and H_C for the present sample (size ~ 4-11 nm) were lesser than the sample prepared by the HMTA route (19-34 nm) due to their smaller dimension.

3.2.5 Mössbauer spectroscopy

Fig. 3.5 shows the Mössbaour spectrum of Fe_3C sample at 300 K. The spectrum was fitted with two sextets and a doublet. The magnitude of the hyperfine field (B_{hf}), isomer shift (δ), quadruple splitting (Δ), line width (Γ), and relative area (R_A) for Fe atoms at two sites are given in Table 3.2. The two sextets had B_{hf} values of 21.05 and 20.92 T, which is attributed to two different atomic positions of iron (Fe) in the orthorhombic unit cell structure for iron carbide. However, the cited B_{hf} magnitudes in the literature are 20.9 and 20.6 T [71, 119].
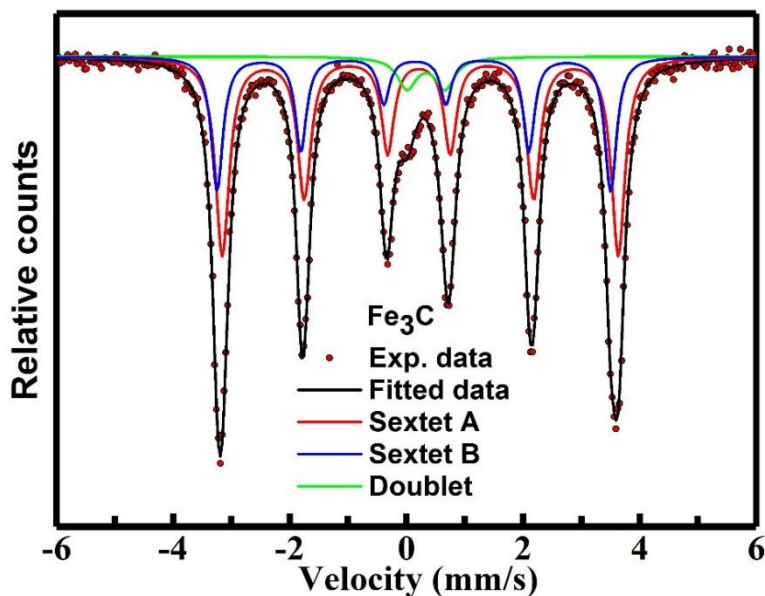

Figure 3.5: The Mössbaur spectrum of Fe_3C nanoparticles recorded at room temperature.

The slight modification in the values might be due to the presence of submicron sized particles. The isomer shift values for the two sextets were 0.22 and 0.13 mm/s. In contrast, the shift values for these two sextets are found to be equal (~ 0.18 mm/s) for the bulk specimen. However, a minor difference in the IS values might be due to its finer size and different synthesis routes. The doublet acquired in the spectrum could be due to the superparamagnetic component in the material associated with the presence of submicroscopic particles.

Table 3.2: Hyperfine parameters magnitudes (B_{hf}, Q_S, IS, and R_A) revealed after fitting of the Mössbauer spectrum of the Fe_3C sample.

Iron site	Hyperfine field (B_{hf}) T ± 0.01	Quadruple splitting, (Δ) mm/s ± 0.02	Isomer shift (δ) mm/s ± 0.01	Outer line width, (Γ) mm/s	Relative Area (R_A) ± 0.03 %	Fitting quality χ^2
Sextet A	21.05	0.024	0.23	0.284	64	
Sextet B	20.92	- 0.017	0.14	0.243	31	1.82
Doublet	-	0.654	0.34	0.395	5	

3.2.6 Investigation of colloidal stability

One of the essential factors relating to biomedical applications is the colloidal stability of ferrofluids which is produced from the aqueous suspension of MNPs. A suitable polymer is generally used as stabilizer. The stability is achieved from the compromise between the forces due to Coulombic attraction, electrostatic and steric repulsions. The zeta potential (ζ) is used to index the colloidal dispersion in aqueous and physiological medium. Here, the carbide nanoparticles were functionalized using a

nonionic tri-block copolymer (pluronic acid, F127), which possesses a central hydrophobic branch of polypropylene oxide (PPO) bordered by two hydrophilic chains of polyethylene oxide (PEO).
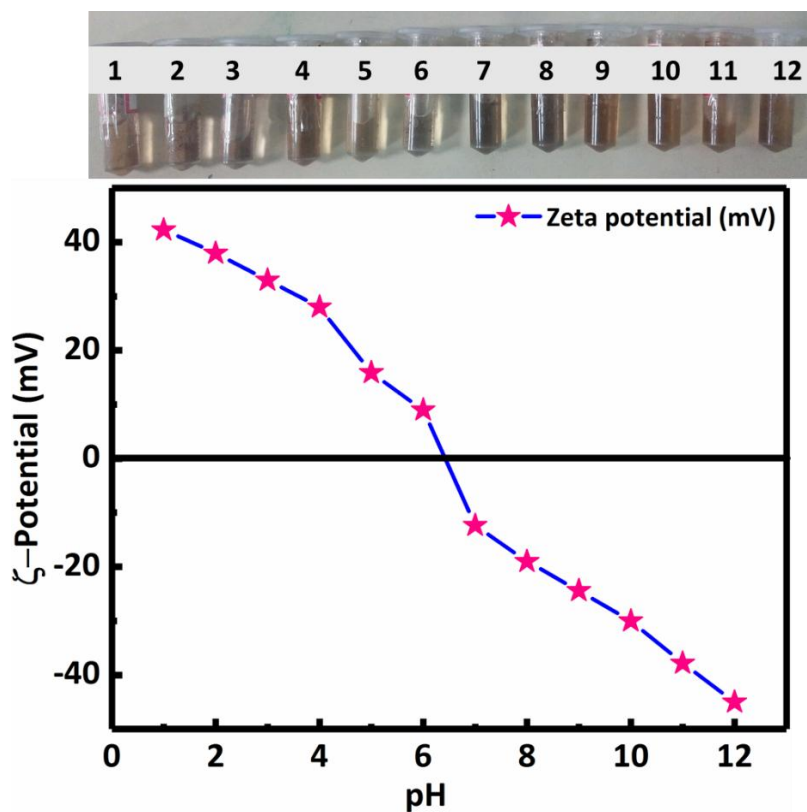

Figure 3.6: Colloidal stability of Fe₃C nanoparticles.

The high negative zeta-potential (ζ) values acquired at the ambient condition is evident of electrostatic contribution for the stabilization of suspension. Figure 3.6 represents the zeta potential values obtained for Fe_3C nanoparticles functionalized with pluronic acid (F-127) and suspended in distilled water with varying pH (1 – 12). The zeta potential values were found to be as 42.3, 38, 33, 28, 15.9, 9, -12.3, -19, -24.4, -30, 37.8 and -45 mV corresponding to the pH values of 1, 2, 3, 4, 5, 5, 7, 8, 9, 10, 11 and 12

respectively. The stability of this ferrofluid is confirmed from the larger zeta potential values (> 35 mV) in highly acidic and highly basic media.

3.2.7 Magnetic hyperthermia studies

For the encapsulation of iron carbide nanoparticles, the copolymer pluronic acid, F127, was used. The homogeneous dispersion of Fe_3C nanoparticles in F-127 was stable for a few days. The hydrophilic non-ionic surfactant, F-127, is a tri-block copolymer consisting of a central hydrophobic block of polypropylene glycol flanked by two hydrophilic blocks of polyethylene glycol (PEG) [147, 148].

It can be stated that the stirring of MNPs with pluronic acid for 24 h at room temperature created a bilayer coating of the acid, which was hydrophilic. The coated sample was separated by a magnet and then distilled water was added into it. The solution was then ultrasonicated with high frequency sonicator. It facilitates the formation of its stable ferrofluid. The prepared ferrofluids had 5, 10, 25, and 50 mg/mL concentration of Fe_3C.

The temperature *vs*. time curves for the Fe_3C MNP_S based ferrofluid display heat generation in the presence of AC magnetic fields having different sets of amplitudes and frequencies (Fig. 3.7 a). For example, at 23 mT and 261 kHz, the sample has shown a higher initial slope for the higher concentration of MNPs. Further, the time consumed to achieve the therapeutic temperature was 361, 310, 408, and 140 s for ferrofluids having 5, 10, 25, and 50 mg/mL of MNPs respectively (Fig. 3.7 a). Further, for the same ferrofluids and at this external field, the stabilization of temperature was observed at 47, 47, 48, and 56 °C respectively (Fig. 3.7 a). This observation was similar to that of

substituted Fe₃O₄ samples. In contrast, at the same concentrations viz. 5, 10, and 25 mg/mL of MNPs, the stabilization of temperature was noticed at 37, 46, and 53 °C at a field of amplitude 25 mT and a frequency of 109 kHz (Fig. 3.7 a). Further, the ferrofluid with the highest concentration of MNPs (i.e. 50 mg/mL) showed a constant increase in the temperature (Fig. 3.7 a).
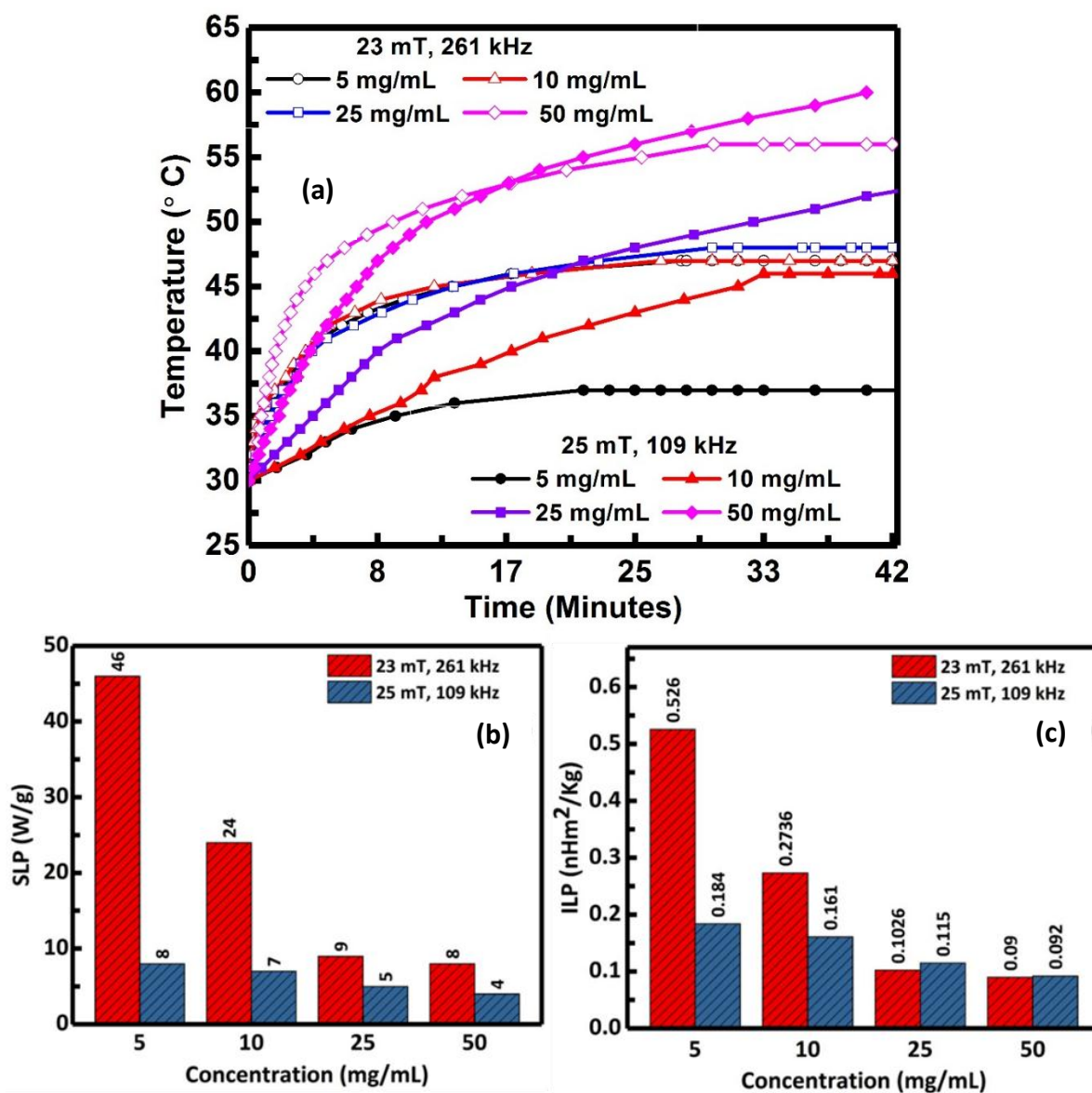

Figure 3.7: (a) Temperatures *vs.* time plots (b) SLP, and (c) ILP values obtained for various concentrations of Fe₃C MNPₛ at two different fields.

The time needed to accomplish the suitable temperature (~ 42 °C) for MHT was observed to be 1320, 690, and 303 s (Fig. 3.7 a) for the ferrofluids having 10, 25, and 50 mg/mL respectively (Fig. 3.7 a). The longer duration to achieve the temperature in the latter field could be due to its lesser frequency. The variation in the SLP values at the given fields for all the ferrofluids are shown in Fig. 3.7 (b). The higher SLP values were obtained at 23 mT, 261 kHz for each concentration of MNPs. It could be accomplished to its higher heating rate (Figs. 3.7 a). Amongst various concentrations, the ferrofluid with 5 mg/mL had the highest SLP values in all fields (Fig. 3.7 b). Nevertheless, the obtained SLP values were higher than that of some of the reported values for iron oxide based MNPs but lesser than of values reported by others [25, 29].

Overall, the SLP values (maximum value = 46 W/g) of Fe_3C suggest that it can be suitably used for MHT application (Fig. 3.7 b). It has been observed that the SLP values for the same material estimated by different scientists show significant deviations. Thus, to have a better comparison, ILPs values for the ferrofluids were estimated. The maximum ILP value for the ferrofluid having a concentration of 5 mg/mL was 0.55 nHm^2/kg at a magnetic field of amplitude 23 mT (Fig. 3.7 c). The SLP and ILP values were analogous with that of iron oxide based ferrofluids. Similar to the SLP values, at a constant field, the ILP values also decreased with increased concentration of MNPs (Fig. 3.7 c).

3.2.8 Biocompatibility study

The *in-vitro* study of Fe_3C MNPs was carried out with A549, a human lung cancer cell lines, using SRB assay. The percentage cells viability of the cells treated with

bare particles as well as ferrofluid is shown in Fig. 3.8. It has been observed that approximately 80-90 % of confluent cells grown without any contamination after the incubation for 24 h (Fig. 3.8 a). Further, the cells treated with MNP$_S$ having a concentration of 1 mg/mL also shown growth similar to that of controlled one (Figs. 3.8 a and b).
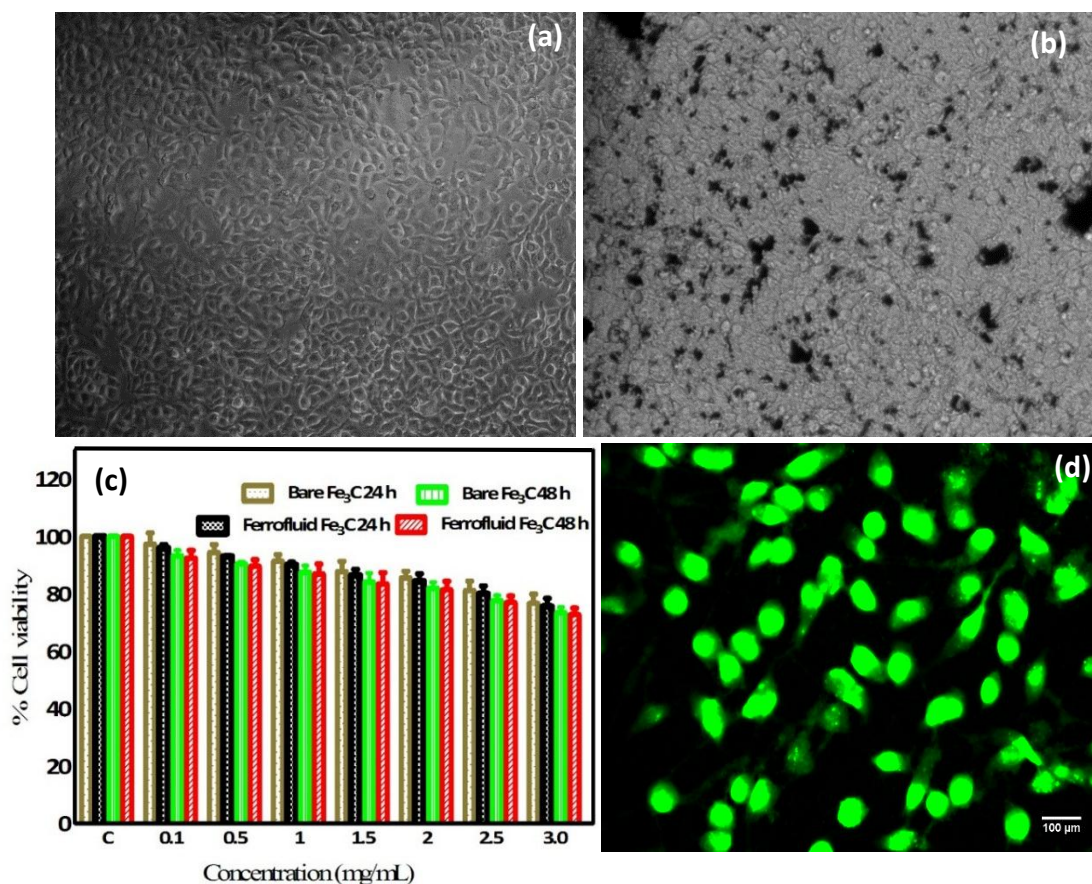

Figure 3.8: Biological study of A549 lung cancer cell lines treated with Fe$_3$C nanoparticles a) control cells growth after 24 h of incubation, b) cells treated with the 1 mg/mL of MNP$_S$ for 24 h, c) % cell viability with bare particles as well as with its ferrofluid at varying concentrations (0.1, 0.5, 1, 1.5, 2, 2.5 and 3 mg/mL) after 24 and 48 h of incubation, and d) fluorescence image of the cells stained with acridine orange .

Nevertheless, the black particles of Fe_3C were found to be spreaded over the cells layer (white). These MNPs were neither damaging the cells mechanically nor chemically (Fig. 3.8 b). Moreover, it can be noticed that the percentage viability continuously decreased with increased concentration of MNPs for both bare particles as well as ferrofluid (Fig. 3.8 c). The % cell viability at lower (0.1 mg/mL) to higher (3 mg/mL) concentration diminished from 97 to 76 for bare particles and 96 to 76 for ferrofluid after the incubation for 24 h. Further, at similar concentrations, after the incubation for 48 h, it was found to be reduced from 93 to 73 for the bare particles and 92 to 73 for the ferrofluids. It can be remarked that there was no significant difference in the cells viability with bare particles or ferrofluid at all concentrations even after 48 h of incubation (Fig. 3.8 c). However, at same concentration there was a slight decrease in the percentage viability with increased incubation period (Fig. 3.8 c). Fluorescence micrograph of the A549 cells was taken after a treatment with ferrofluid having a concentration of 1 mg/mL of MNPs-for 24 h (Fig. 3.8 d). It can be stated that the cells had healthy growth even in the presence of MNP_S, which was supported by the SRB assay.

3.3 Conclusions

The single phase Fe_3C nanoparticles having a size around 4-11 nm was obtained by a sol-gel assisted route. Both X-ray diffraction and transmission electron microscopy findings confirmed this. In addition, X-ray photoelectron and Mössbauer spectroscopy supported this conclusion. The value of M_S for this sample was either comparable or more than its corresponding oxides. The SLP and ILP magnitudes were relatively higher at lesser contents of MNPs. The maximum magnitudes for SLP and ILP were 46 W/g

and 0.526 nHm^2/kg respectively at 23 mT. Thus, we can argue that these MNP$_S$ based ferrofluids may be a possible replacement of magnetic iron oxides. The % cell viability was observed to be nearly 87 at a concentration of 1 mg/mL. Hence, it can be concluded that Fe$_3$C MNP$_S$ may be explored for various bioapplications including MHT, due to its better magnetic properties and biocompatibility.